

Insights into elastic properties of coarse-grained DNA models: q -stiffness of cgDNA vs. cgDNA+

Wout Laeremans,^{1,2,3} Midas Segers,² Aderik Voorspoels,² Enrico Carlon,^{2, a)} and Jef Hooyberghs^{3, b)}

¹⁾*Soft Matter and Biological Physics, Department of Applied Physics, and Institute for Complex Molecular Systems, Eindhoven University of Technology, P.O. Box 513, 5600 MB Eindhoven, Netherlands*

²⁾*Soft Matter and Biophysics Unit, KU Leuven, Celestijnenlaan 200D, 3001 Leuven, Belgium*

³⁾*UHasselt, Faculty of Sciences, Data Science Institute, Theory Lab, Agoralaan, 3590 Diepenbeek, Belgium*

(Dated: January 11, 2024)

Coarse-grained models have emerged as valuable tools to simulate long DNA molecules while maintaining computational efficiency. These models aim at preserving interactions among coarse-grained variables in a manner that mirrors the underlying atomistic description. We explore here a method for testing coarse-grained vs. all-atom models using stiffness matrices in Fourier space (q -stiffnesses), which are particularly suited to probe DNA elasticity at different length scales. We focus on a class of coarse-grained rigid base DNA models known as cgDNA and its most recent version cgDNA+. Our analysis shows that while cgDNA+ follows closely the q -stiffnesses of the all-atom model, the original cgDNA shows some deviations for twist and bending variables which are rather strong in the $q \rightarrow 0$ (long length scale) limit. The consequence is that while both cgDNA and cgDNA+ give a suitable description of local elastic behavior, the former misses some effects which manifest themselves at longer length scales. In particular, cgDNA performs poorly on the twist stiffness with a value much lower than expected for long DNA molecules. Conversely, the all-atom and cgDNA+ twist is strongly length scale dependent: DNA is torsionally soft at a few base pair distances, but becomes more rigid at distances of a few dozens base pairs. Our analysis shows that the bending persistence length in all-atom and cgDNA+ is somewhat overestimated.

I. INTRODUCTION

All-atom simulations have played a fundamental role in our understanding of DNA mechanics. Despite remarkable advances in computing power, such simulations are still limited to sequences of few tens of base pairs (bp) and to times spanning about $1 \mu\text{s}$. Sometimes advanced sampling techniques can be used to alleviate some of these limitations by simulating rare events and extreme conformations²⁻⁶. However, the large computational cost remains a heavy burden. When atomistic details are not of crucial importance, coarse-grained models⁷⁻¹² represent a valid alternative to all-atom simulations as they can handle 100 – 1000 bp long molecules for considerably longer time scales. In these models, lower-resolution, coarse-grained beads interact with each other through potentials that are parametrized to reproduce the thermodynamic, structural, and mechanical properties of DNA. Several coarse-grained DNA models neglect sequence dependent effects, but can be used to explore conformational changes, strand dissociation/hybridization, supercoils formation and other effects¹³⁻¹⁷.

A very good account of sequence-dependent effects is given by coarse-grained rigid base DNA models^{18,19}. Such models describe bases as rigid bodies and a DNA conformation by means of rotations and translation between the rigid units, see Fig. 1. The rigid base models describe DNA molecules in their canonical B-form and at a fixed temperature, the base pairs do not dissociate and self-avoidance effects are not included. The interactions between the rigid bases are usually

encoded by harmonic potentials^{18,19} and can be represented by a stiffness matrix. Recently also multimodal interactions were proposed²⁰. The standard cgDNA model¹⁸ parametrizes the DNA conformations using the canonical twelve coordinates, defined by the Tsukuba convention²¹. Six of these are intra base pair coordinates (buckle, propeller, opening, shear, stretch, stagger) and six are inter base pair (or junction) coordinates (tilt, roll, twist, shift, slide, rise). In the more recent cgDNA+^{19,22} the phosphate groups are treated explicitly, which brings the number of coordinates to 24 per bp, see Fig. 1. The parameters of the cgDNA/cgDNA+ models were tuned to all-atom simulations that are used as references. For this purpose, the model stiffness matrix was determined by minimizing the distance between the associated covariance matrix of the model and that of the all-atom simulations²³.

The focus of this paper is on mechanical properties of DNA that involve couplings beyond nearest-neighbor sites, following recent work along this line^{24,25}. For this purpose we study the stiffness of cgDNA and cgDNA+ in Fourier space (q -stiffness) and compare it with all-atom simulations. Such quantities provide considerable insights about the elastic properties of the molecule at different length scales²⁴. We show that some degrees of freedom are stiffer/softer at the base pair level, as compared to the long wavelength limit ($q \rightarrow 0$), describing the asymptotic stiffness of very long molecules. Our analysis shows that cgDNA+ considerably improves over the earlier version cgDNA. The cgDNA+ model shows a remarkable quantitative agreement with all-atom data for all q -stiffnesses of the twelve inter- and intra-bp coordinates. Besides the specific analysis of rigid base models, this work provides a methodological example for testing coarse-grained DNA models via q -stiffnesses. This paper is organized as follows. Section II reviews the main properties of the rigid base

^{a)}Electronic mail: enrico.carlon@kuleuven.be

^{b)}Electronic mail: jef.hooyberghs@uhasselt.be

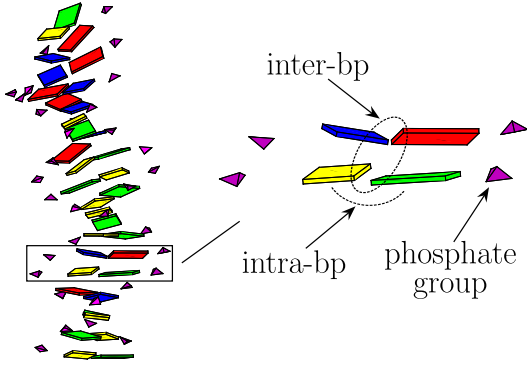


Figure 1. Rigid base models (as cgDNA¹⁸) represent bases in each B-DNA molecule as rigid objects, here plotted as rectangles with the following color code: A (red), T (blue), C(yellow) and G(green). In the original cgDNA-model, a DNA conformation is described by 12 coordinates, 6 of which are intra-bp coordinates and 6 inter-bp coordinates, parametrizing rotations and translations about the rigid units. The image shows a rigid base model conformation sampled from cgDNA+^{19,22}, which takes explicitly into account phosphate groups, here shown as purple pyramids.

model and introduces the stiffnesses in Fourier space, also referred to as q -stiffnesses, which are computed and discussed in Sec. III. Section IV links the q -stiffnesses to length scale dependent elasticity, focusing on torsional and bending persistence lengths. Section V focuses on the real-space two-point correlation function of several rigid base parameters and their associated q -stiffness. Section VI discusses the results obtained and presents some conclusions.

II. RIGID BASE MODELS

We consider here a description based on the canonical rigid base coordinates introducing a twelve dimensional vector Δ_n , with $n = 0, 1, \dots, N-1$ labeling the sites along the sequence. The elements of the vector Δ_n represent the deviation of the twelve rigid base coordinates with respect to their average values, such that $\langle \Delta_n \rangle = 0$, with $\langle \cdot \rangle$ denoting thermal averaging. Small deformations from equilibrium are usually described within the harmonic approximation²⁶, with an energy given by

$$\beta E = \frac{a}{2} \sum_n \sum_m \Delta_n^\dagger M_m^{(n)} \Delta_{n+m}, \quad (1)$$

with $\beta = 1/k_B T$ the inverse temperature, k_B the Boltzmann constant and a the average distance between consecutive base pairs ($a = 0.34$ nm for DNA). $M_m^{(n)}$ are 12×12 stiffness matrices and depend on the sequence composition, reflected in the dependence on the site index n . The above model allows for distal couplings between variables at distinct sites n and $n+m$.

As our primary interest will be to highlight the nature of the distal couplings, we will neglect sequence dependent effects and ignore the n dependence in $M_m^{(n)}$. Assuming an effective translationally invariant DNA model (obtained by averaging

over different sequences) it is convenient to introduce a discrete Fourier transform of the canonical rigid base coordinates as follows

$$\tilde{\Delta}_q = \sum_{n=0}^{N-1} \Delta_n e^{-2\pi i q n / N}, \quad (2)$$

where $q = -(N-1)/2, -(N-3)/2, \dots, (N-3)/2, (N-1)/2$ (for N odd). As the vector Δ_n is real, complex conjugation gives $\tilde{\Delta}_q^* = \tilde{\Delta}_{-q}$. The model (1) in q -space then takes the form

$$\beta E = \frac{a}{2N} \sum_q \tilde{\Delta}_q^\dagger \tilde{M}_q \tilde{\Delta}_q, \quad (3)$$

where \dagger denotes Hermitean conjugation and where the matrix \tilde{M}_q is obtained by taking the Fourier transform of M_m ²⁴

$$\tilde{M}_q = \sum_m M_m e^{-2\pi i q m / N}. \quad (4)$$

The assumed translational invariance for a finite system only applies with periodic boundary conditions. The open DNA molecule will also have additional boundary terms, which do not influence the large N bulk behavior. The matrix \tilde{M}_q is 12×12 and, for convenience, we organize it in 16 submatrices as follows

$$\tilde{M}_q \equiv \begin{bmatrix} \tilde{A}_q & \tilde{B}_q & \tilde{C}_q & \tilde{D}_q \\ \tilde{E}_q & \tilde{F}_q & \tilde{G}_q & \tilde{H}_q \\ \tilde{I}_q & \tilde{J}_q & \tilde{K}_q & \tilde{L}_q \\ \tilde{N}_q & \tilde{O}_q & \tilde{P}_q & \tilde{Q}_q \end{bmatrix}. \quad (5)$$

where $\tilde{A}_q, \tilde{B}_q \dots \tilde{Q}_q$ are 3×3 matrices. The order of the 12 coordinates is chosen to be: tilt, roll, twist, shift, slide, rise, buckle, propellor, opening, shear, stretch, stagger. For example, the first element on the diagonal of \tilde{F}_q is the q -stiffness of the ‘‘shift’’ variable. The elements 1 to 6 and 7 to 12 correspond to inter- and intra-bp coordinates, respectively. Off-diagonal elements are cross-coupling terms between different coordinates as e.g. ‘‘shift-slide’’ or ‘‘roll-twist’’. The stiffness matrix can be obtained from the inversion of the covariance matrix²⁴

$$\tilde{M}_q = \frac{N}{a} \langle \tilde{\Delta}_q \tilde{\Delta}_q^\dagger \rangle^{-1}, \quad (6)$$

where, in our case, $\tilde{\Delta}_q$ is obtained from simulations. $\tilde{\Delta}_q$ and $\tilde{\Delta}_q^\dagger$ are 12-dimensional column and row vectors. The product in (6) gives a 12×12 matrix. The Monte Carlo (cgDNA/cgDNA+) sampling or the molecular dynamics (MD) simulations (all-atom) produces real space configurations expressed in terms of the 12 canonical coordinates. For every simulated sample, this gives a vector Δ_n for each site $n = 0, 1, \dots, N-1$ of the DNA sequence. These are Fourier transformed to give $\tilde{\Delta}_q$. Using Eq. (6), the matrix \tilde{M}_q is deduced. In general, the elements of \tilde{M}_q have real and imaginary parts. From Eq. (4), it follows that the real part of the elements of q are symmetric in q , while the imaginary parts are antisymmetric.

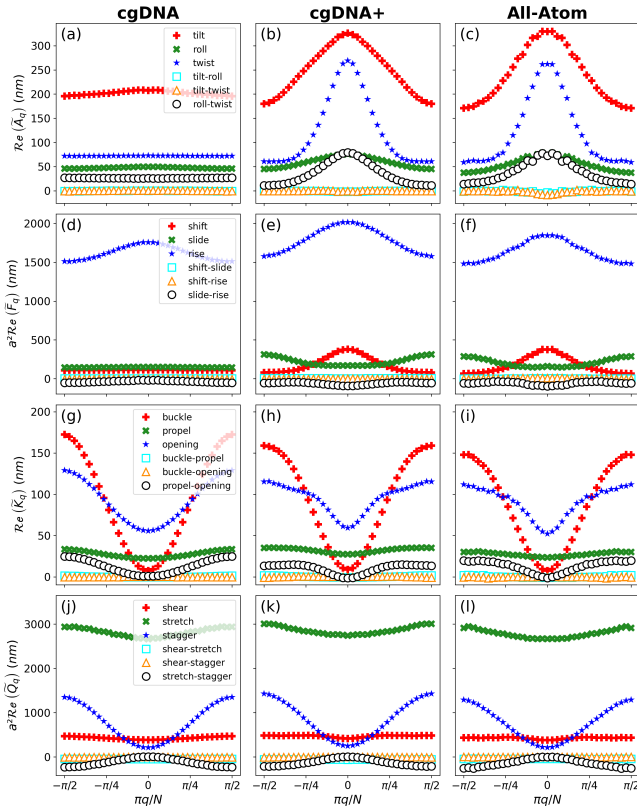


Figure 2. Real part of q -stiffnesses of inter- and intra-basepair degrees of freedom obtained from Monte Carlo sampling the cgDNA and cgDNA+ models and all-atom MD simulations (left, center and right columns, respectively). The sub-blocks \tilde{A}_q , \tilde{F}_q , \tilde{K}_q and \tilde{Q}_q of \tilde{M}_q are shown (5). Stiffnesses of translational degrees of freedom (\tilde{F}_q , \tilde{Q}_q) are rescaled by a factor a^2 ($a = 0.34$ nm) in order to express stiffnesses in units nm in all plots. cgDNA+ stiffnesses are in very good agreement with MD simulations. The largest differences between cgDNA and cgDNA+ are for tilt and twist coordinates (block \tilde{A}_q , (a,b,c)). cgDNA lacks the peak at $q = 0$ for tilt, twist and twist-roll couplings, which is present in cgDNA+ and all-atom data.

III. q -STIFFNESS IN CGDNA(+) VS. MD SIMULATIONS

Figure 2 shows a plot of the real parts of the elements of \tilde{A}_q , \tilde{F}_q , \tilde{K}_q and \tilde{Q}_q , the four 3×3 diagonal sub-block matrices of \tilde{M}_q which was obtained from Eq. (6). The three columns report the data from cgDNA, cgDNA+ and all-atom simulations which are obtained from averaging over two different sequences, see details in Appendix A. The cgDNA/cgDNA+ data are generated using a Monte Carlo sampling, while the all-atom data are from averaging a 100 ns MD simulation (data from²⁷). There is a remarkable agreement here between cgDNA+ and all-atom data, and a considerable improvement from cgDNA to cgDNA+ for some, but not for all, matrix elements. The strongest differences between cgDNA and cgDNA+ is in the twist and bend (tilt/roll) coordinates, which are in the block \tilde{A}_q and shown in Fig. 2(a,b,c). For these coordinates the cgDNA stiffnesses are very weakly q -dependent,

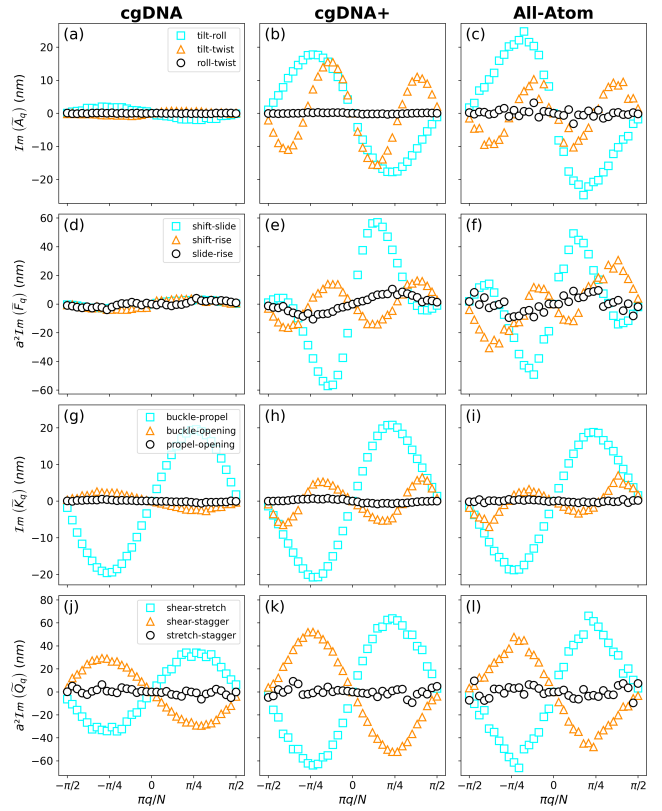


Figure 3. Imaginary part of q -stiffnesses of rigid base coordinates for cgDNA/cgDNA+ and all-atom simulations, showing the same sub-blocks of the stiffness matrix as in Fig. 2. Similar to the real counterparts, the imaginary parts of the cgDNA+ stiffnesses (middle column) are in excellent agreement with all-atom MD simulations (right column), whereas the cgDNA-model does not reproduce all-atom data. The lack of structure is most notably for the inter-basepair coordinates (a-f).

while a strong dependence for tilt and twist is observed in the cgDNA+ and the all-atom data.

Large variations in stiffnesses for different q indicate that the elastic response of the molecule strongly depends on the length scale at which it is probed^{24,28,29}, as discussed in more details in Sec. IV. For tilt and twist, cgDNA fits well the short scale behavior which corresponds to $|q| \approx N/2$, i.e. the two edges of the graphs in Fig. 2. However, the cgDNA data lacks the sharp peaks at $q = 0$ found in cgDNA+ and all-atom simulations (b,c). The $q = 0$ corresponds to the long length scale behavior, as discussed in Sec. IV. The good agreement between the q -stiffnesses of cgDNA and cgDNA+ at $|q| \approx N/2$ stems from the fitting of local couplings of the all-atom data. To improve cgDNA, i.e. to reproduce the q -dependence observed in all-atom data, one would need to account for distal components by adding non-vanishing matrix elements in M_m in (4). These effective distal couplings are generated via the integration of phosphate coordinates in cgDNA+.

Figure 2(d,e,f) compare the translational inter-bp stiffnesses. While there is good agreement in all three models for the rise stiffness (the stiffer of the translational inter-bp

coordinate), the cgDNA+ and all-atom data show remarkable similarity in the q -dependence for slide and shift. Stiffnesses of intra-bp coordinates (Fig. 2(g-l)) for all three models are in good agreement with each other, which indicates that the additional phosphate degrees of freedom of cgDNA+ have a weak effect on the intra-bp coupling. Nevertheless, some minor differences in shape can be observed, most visible in case of the opening stiffness. We note that there are two different types of q -dependences in Fig. 2. Some stiffnesses have a maximum at $q = 0$ (inter-bp couplings (a-f)), while others have a minimum at $q = 0$ (intra-bp couplings (g-l)). A maximum at $q = 0$ indicates that the corresponding coordinate is soft at short scale and becomes stiffer at longer scales, while the opposite is true for a minimum at $q = 0$.

Figure 3 shows a plot of the imaginary parts of the blocks $\tilde{A}_q, \tilde{F}_q, \tilde{K}_q$ and \tilde{Q}_q , of the matrix \tilde{M}_q . Symmetry imposes vanishing imaginary part to all diagonal elements, hence only the three off-diagonal components of each block matrix are shown in the plots of Fig. 3. Similarly to their real counterparts in Fig. 2, we note a much weaker q -dependence for cgDNA as compared to cgDNA+ and all-atom data. The weak q -dependence in cgDNA is again very striking for the elements of the blocks \tilde{A}_q and \tilde{F}_q , depicting the stiffnesses of the inter-bp coordinates (see plots (a-f)). Again cgDNA+ and all-atom data appear to be in excellent agreement with each other.

IV. LENGTH-SCALE DEPENDENT ELASTICITY

A model characterized by a q -dependent stiffness has elastic properties which depend on the length scale at which they are probed²⁴. In this section we elaborate on the twist and bending properties. To introduce the concept we evaluate the response of the system to a pure twist perturbation. We start with the partition function Z and focus on the excess twist, which we denote with $\tilde{\Omega}_q$, by integrating out all other eleven variables in the rigid base model. This gives

$$Z = \int \prod_q d\tilde{\Delta}_q e^{-\frac{a}{2N} \sum_q \tilde{\Delta}_q^\dagger \tilde{M}_q \tilde{\Delta}_q} = \int \prod_q d\tilde{\Omega}_q e^{-\beta E_{\text{twist}}}. \quad (7)$$

As the full model is Gaussian, the integration over all degrees of freedom but twist gives an effective one dimensional model for twist elasticity which is still Gaussian. The energy is thus quadratic in $\tilde{\Omega}_q$ and takes the form

$$\beta E_{\text{twist}} = \frac{a}{2N} \sum_q \tilde{\mathcal{C}}_q |\tilde{\Omega}_q|^2, \quad (8)$$

where the scalar $\tilde{\mathcal{C}}_q$ is the stiffness of the mode q . We note that in general $\tilde{\mathcal{C}}_q \neq (\tilde{M}_q)_{33}$ because of off-diagonal couplings between twist and other coordinates. More precisely, $\tilde{\mathcal{C}}_q$ can be obtained as a Schur complement of the 12×12 stiffness matrix \tilde{M}_q ^{22,29}.

A physical way to probe the length-scale dependent twist response is to apply a torque τ to a sub-sequence of m base

pairs. The energy of the system gets an extra term and becomes, in real space coordinates,

$$\beta E^\tau = \beta E_{\text{twist}} - \beta \tau a \sum_{n=1}^m \Omega_n, \quad (9)$$

with $a \sum_{n=1}^m \Omega_n$ the total excess twist angle of the DNA segment of m base pairs. To calculate the partition function Z for (9) it is convenient to switch to Fourier space coordinates $\tilde{\Omega}_q$, presented in previous work²⁴. The total free energy $F = -k_B T \log Z$ is then given by

$$F(\tau) = F_0 - \frac{m\beta\tau^2}{2\mathcal{E}_m}, \quad (10)$$

where \mathcal{E}_m is introduced as the variable of interest: the torsional stiffness related to a torque applied to m subsequent base pairs. Note that the free energy (10), as an extensive quantity, contains a torque response term proportional to m . The crucial point here is that in general \mathcal{E}_m depends on m : the torsional stiffness depends on the length scale m at which the twist elasticity is probed. The torsional stiffness is given by (the details of the derivation can be found in²⁴)

$$\begin{aligned} \frac{1}{\mathcal{E}_m} &= \frac{a}{m\pi} \int_{-\pi/2}^{+\pi/2} \frac{\sin^2 my}{\sin^2 y} \frac{\langle |\tilde{\Omega}_q|^2 \rangle}{N} dy \\ &= \frac{1}{m\pi} \int_{-\pi/2}^{+\pi/2} \frac{\sin^2 my}{\sin^2 y} \frac{dy}{\tilde{\mathcal{C}}_q}, \end{aligned} \quad (11)$$

where we introduced the rescaled momentum $y = \pi q/N$ and replaced the discrete sum in q with a continuous integral, assuming $N \rightarrow \infty$. The asymptotic behavior $m \gg 1$ of (11) has been discussed in prior work³⁰ and it is given by

$$\mathcal{E}_m = \frac{m}{m+A} \tilde{\mathcal{C}}_{q=0} + \mathcal{O}(e^{-m/\lambda}), \quad (12)$$

with A a scale factor. Apart from an exponentially small correction, \mathcal{E}_m has a leading algebraic $1/m$ decay to $\tilde{\mathcal{C}}_{q=0}$. At long length scales ($m \rightarrow \infty$) the integrand in (11) is increasingly peaked around $y = 0$, hence the torsional stiffness of an infinitely long chain is that of the mode $q = 0$.

With this concept in place, we analyzed the torsional stiffness \mathcal{E}_m of the cgDNA and cgDNA+ models. Figure 4(a) summarizes the results. The dashed lines show the stiffness obtained from a numerical integration of (11). As a comparison, the solid lines were obtained from real space data, not by applying a torque, but from the correlation function²⁴ $\langle \cos(\sum_{i=n}^{n+m-1} a\Omega_i) \rangle = e^{-am/(2\mathcal{E}_m)}$, averaging over 100 independent sequences of length 500 bp. Both the cgDNA and cgDNA+ model show an explicit m -dependence, they have similar values of the stiffnesses at the shortest length scale ($m = 1$). For high m -values the curves obey equation (12) and decay to an asymptotic \mathcal{C} -value listed in Table I. cgDNA+ shows a strong length-scale dependence reaching asymptotically a value which is close to (about 20% higher) the value $\mathcal{C} = 110$ nm measured in single molecule magnetic tweezers (MT) experiments³¹⁻³³. These experimental values can be considered as the high- m limit since such devices measure the

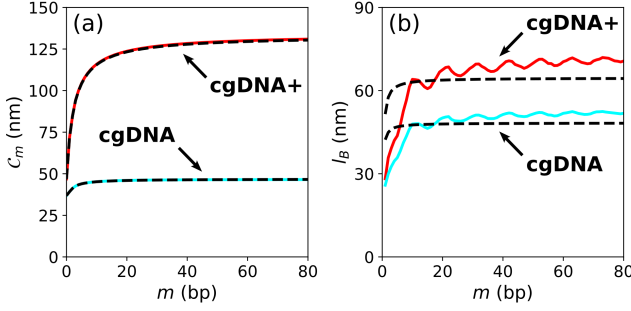


Figure 4. (a) Solid lines: Torsional stiffness for $cgDNA$ and $cgDNA+$, obtained from the twist correlation function $\langle \cos(\sum_{i=n}^{n+m-1} a\Omega_i) \rangle = e^{-am/(2\mathcal{C}_m)}$ averaging over 100 random sequences with length 500 bp. Dashed lines: Data obtained from the numerical integration of (11). (b) Solid lines: Bending persistence length calculated for $cgDNA$ and $cgDNA+$ from the tangent-tangent correlation function $\langle \hat{t}_n \cdot \hat{t}_{n+m} \rangle = e^{-am/l_B(m)}$, with \hat{t}_n the unit tangent vector at site n . Dashed lines: Bending persistence length l_B as obtained from the numerical integration of (13). We notice a difference between the two estimates, whose origin is discussed in the text. The extrapolated bending persistence length of $cgDNA+$ is above the consensus value $l_B \approx 50$ nm, while the $cgDNA$ value is rather consistent with experiments. As in (a) the DNA appears to be stiffer at longer scales.

torsional response of a several Kbp long molecule, using a magnetic bead attached to one of its ends, while its other end is attached to a solid surface. $cgDNA$ instead, shows a much weaker length dependence of the torsional stiffness, with an asymptotic value $\mathcal{C}_{m \rightarrow \infty} = 47$ nm, which is well-below the experimental results.

We now discuss length-scale dependence of bending deformations. In Ref. 24 the following expression for the bending persistence length l_B was derived

$$\frac{1}{l_B} = \frac{a}{m\pi} \int_{-\pi/2}^{+\pi/2} \frac{\sin^2 my}{\sin^2 y} \frac{\Psi_{q+\Delta q} + \Psi_{q-\Delta q}}{N} dy, \quad (13)$$

in which again $y = \pi q/N$ and

$$\Psi_q = \frac{1 - \cos(a\omega_0)}{2(a\omega_0)^2} \langle |\tilde{\tau}_q|^2 + |\tilde{\rho}_q|^2 \rangle, \quad (14)$$

where $\tilde{\tau}_q$ and $\tilde{\rho}_q$ are the Fourier transform of the tilt and roll variables (the two bending modes), $\omega_0 = 1.76$ nm⁻¹ is the average intrinsic twist and $\Delta q \equiv Na\omega_0/(2\pi)$. Equation (13) has a similar m -dependence as (11), but there are some differences. The bending in DNA is described by two components: the (stiffer) tilt $\tilde{\tau}_q$ and the (softer) roll $\tilde{\rho}_q$. In addition (13) contains ω_0 (both explicitly and via Δq) since the DNA frame rotates with the intrinsic twist and this needs to be taken into account in the calculation of l_B . The expression (13) was derived under the assumption that the roll and tilt angles are small compared to the intrinsic twist angle which is $\approx 34^\circ$ (an approximation referred to as intrinsic twist dominance²⁴).

Figure 4(b) shows a plot of the numerical estimate of (13) for $cgDNA$ and $cgDNA+$ (dashed lines). Length scale effects

are here much weaker as compared to those observed in the torsional stiffness of Fig. 4(a). As for the twist, also in bending the DNA appears to be softer at short length scales and asymptotically stiffer as $m \rightarrow \infty$, as also observed in other coarse-grained DNA models²⁴. Again $cgDNA+$ is stiffer than $cgDNA$ at high length scales. The weaker m -dependence of l_B is due to the fact that the integrand Ψ_q in (13) depends very weakly on q . As $\int \sin^2(my)/\sin^2(y)dy = m\pi$ a weak q -dependence leads to a weak m -dependence of l_B . Bending fluctuations are dominated by the softer roll, i.e. $|\tilde{\rho}_q| \gg |\tilde{\tau}_q|$. As opposed to tilt, roll fluctuations very weakly depend on q , which is a typical feature of double stranded polymers²⁵. We have also computed the bending persistence length via decay of the tangent-tangent correlation functions

$$\langle \hat{t}_n \cdot \hat{t}_{n+m} \rangle = e^{-am/l_B(m)}. \quad (15)$$

The data for l_B vs. base pair distance m thus obtained are shown as solid lines in Fig. 4(b). There is a noticeable difference in the extrapolated l_B from (13) and (15), with the former underestimating the persistence length. This discrepancy was observed previously²⁴ and the oscillatory behavior of the latter method stems from the helicity of the traced contour. The extrapolated data for $cgDNA/cgDNA+$, as well as the experimental value of l_B are given in Table I.

One can notice that the asymptotic value found for the persistence length in case of $cgDNA+$ goes above the usually accepted value of $l_B \approx 50$ nm. This could be expected, as it was reported before that $cgDNA$ predicts a persistence length that is slightly higher than experimental values³⁴. Since we showed that $cgDNA+$ behaves stiffer at the long scale concerning the bending modes, this comes as no surprise. It is important to mention that although the bending persistence length of $cgDNA+$ is asymptotically deviating from the experimental value, the $cgDNA+$ curve is consistent with all-atom data²⁴ when both are evaluated with Eq. (13). This can be seen for the asymptotic value in Table I.

V. DISTAL SITES CORRELATIONS

The non-local couplings induce correlations between coarse-grained variables defined at DNA distal sites n and $n+m$. These correlations can be linked to the q -stiffness. We illustrate this for the twist-twist correlation function, which via the discrete Fourier transform (3) can be written as

$$\langle \Omega_n \Omega_{n+m} \rangle = \frac{1}{N^2} \sum_q \langle |\tilde{\Omega}_q|^2 \rangle e^{-2\pi imq/N} = \frac{1}{N} \sum_q \frac{e^{-2\pi imq/N}}{a\tilde{\mathcal{C}}_q}, \quad (16)$$

where we have used the equipartition relation analogous to (6) to link twist fluctuations of the mode q to $\tilde{\mathcal{C}}_q$. The latter, as in (8), is the twist stiffness of the mode q obtained from integrating out all other coarse-grained coordinates. We note that (16) is different from the twist correlation function discussed above and defined as the average of the cosine of the twist angle (see caption of Fig. 4). The latter does not vanish even in absence of non-local couplings, while in that case $\tilde{\mathcal{C}}_q$ is q -independent

	cgDNA	cgDNA+	All-Atom	Experiments
\mathcal{C}	47 / 47	134 / 133	125	110 ± 10
l_B	53 / 48	72 / 65	61	45 ± 5

Table I. Asymptotic values (data in nm) of the torsional stiffness \mathcal{C} and of the bending persistence length l_B as obtained from extrapolation of cgDNA/cgDNA+ simulations vs. all-atom²⁴ and experimental data. The measured DNA bending persistence length is salt dependent and at physiological salt concentration ~ 150 nM NaCl is about $l_B = 45 \pm 5$ nm³⁵. The torsional stiffness was measured by several groups with slightly different results^{31–33} and found to be salt independent. The value and error bar reported in the Table ($\mathcal{C} = 110 \pm 10$ nm) covers the range of literature values^{31–33}. For the MC simulations of cgDNA/cgDNA+ 100 random sequences of length 500 bp were used. For cgDNA/cgDNA+, the first value represents the stiffness found from the correlation functions (full lines in Fig. 4), while the second values is obtained from numerical integration (dotted lines in Fig. 4). These asymptotic stiffnesses were obtained by fitting the curves using Eq. (12), where the initial data points ($m < 20$) were excluded from the fit to probe the long length scales, as well as the final ones ($m > 300$) to exclude boundary effects. The all-atom values were taken from Ref. 24, which were obtained only by numerical integration.

and the last term in (16) becomes a sum over q of exponential phases $\exp(-2\pi imq/N)$ which vanishes for any $m \neq 0$. The asymptotic decay of (16) is governed by the leading pole of $\tilde{\mathcal{C}}_q$, i.e. the solution of $\tilde{\mathcal{C}}_q = 0$ with the smallest imaginary part²⁷. Such equation cannot have a real solution $q = q^*$ as this would imply an unstable mode. The most generic pole is of the form

$$\frac{2\pi q_E}{N} = \phi \pm \frac{i}{\xi_E}, \quad (17)$$

which leads to the following asymptotic, damped oscillatory decay of the normalized correlator²⁷

$$\frac{\langle \Omega_n \Omega_{n+m} \rangle}{\langle \Omega_n^2 \rangle} \stackrel{m \gg 1}{\sim} \cos(m\phi + \phi_0) e^{-m/\xi_E}, \quad (18)$$

with ϕ_0 a phase factor. The real part of the leading pole (17) gives the oscillation frequency, while the imaginary part is the inverse decay length, hence the pole with the smallest imaginary part corresponds to the slowest decaying mode.

Figure 5 shows (a) the normalized twist-twist correlator (18) and (b) the corresponding twist stiffness $\tilde{\mathcal{C}}_q$ for cgDNA+. As a comparison, we also show in Fig. 5 the normalized correlator and associated stiffness for two other intra-bp variables: stagger (c,d) and propeller twist (e,f). The stagger is the relative displacement of the two bases forming a base pair along the double helix axis. The propeller twist is the relative rotation angle of the two bases in a base pair. In all three cases shown, the correlator decay reflects the stiffness behavior. In first approximation, the poles real part corresponds to the minimum of the stiffness. In the twist, stagger and propeller twist cases the minimum would give $\phi = \pi$, $\phi = 0$ and $\phi \approx \pi/3$. The first case corresponds to a correlator decay modulated by a factor $\cos(m\pi) = (-1)^m$, i.e. an alternated sign. The second case ($\phi = 0$) leads to a monotonous decay, while the third

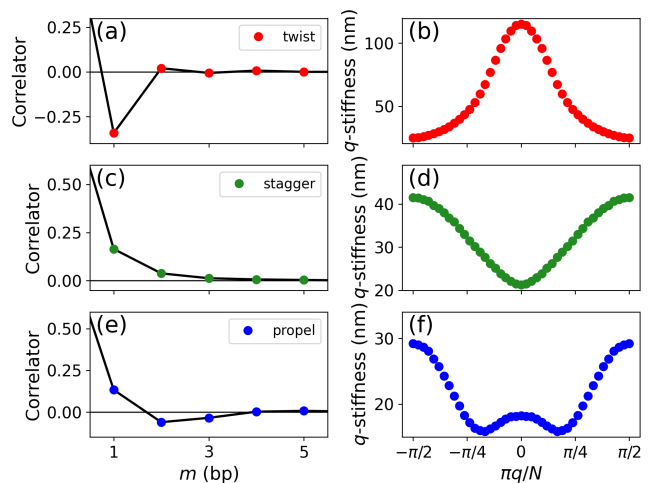


Figure 5. (a,c,e) Normalized real-space correlation function for various degrees of freedom as obtained from cgDNA+ for a 44-mer. (b,d,f) Corresponding q -stiffness spectra. The q -stiffnesses are obtained for each variable separately (see Tab. II), e.g. they are Schur-complements of the 12×12 matrix in Eq. (5) by projecting the 12-dimensional configuration space onto a single dimension.

case ($0 < \phi < \pi$) would correspond to an oscillating decay. The correlators plotted in Fig. 5(a,c,e) reproduce indeed these three distinct behaviors.

We note that correlators rapidly decay and virtually vanish at the distance of $m = 4$ bp. Such correlations potentially generate effective interactions at distal sites which are linked to allosteric effects²⁷. Experiments have shown that proteins binding at distal DNA sites interact with each other via the linker DNA^{36,37}. The characteristic decay length observed in experiments is about ~ 15 bp, which is about one order of magnitude larger than the decay shown in Fig. 5(a,c,e). This discrepancy suggests that distal correlations in DNA are stronger than all-atom simulations (and cgDNA+) currently predict²⁷.

VI. DISCUSSION

In this paper we have analyzed the properties of a class of coarse-grained DNA models known as cgDNA¹⁸ and the most recent improved version cgDNA+^{19,22}. In these models each base is treated as a rigid object. Translations and rotations between two bases forming a base pair are parametrized by six intra-bp coordinates, while relative orientations between consecutive base pairs are defined by another set of six inter-bp coordinates, see Fig. 1. In this way each site in cgDNA is parameterized by 12 coordinates, for cgDNA+ phosphate interactions are added which brings it to 24 coordinates per site²². We compared the two models by integrating out the phosphate contribution of cgDNA+ focusing on the calculation of the 12×12 stiffnesses matrix in Fourier space \tilde{M}_q . The q -dependence of the elements of the stiffness matrix reflects the existence of distal couplings, e.g. coupling between non-proximal sites^{24,25,29}.

Our analysis shows that cgDNA+ is a significant improvement of cgDNA in several aspects. As illustrated in Fig. 2(a-c), the tilt- and twist coordinates of cgDNA+ show a high level of overlap with all-atom data over the whole q -stiffness range. This means that cgDNA+ accurately encodes both the short and long length-scale behavior of the all-atom simulations. The cgDNA model on the other hand, only captures the short length scale of tilt and twist. The improvement of cgDNA+ in twist behavior is especially outspoken, with the torsional stiffness data showing a very strong length-scale dependence (Fig. 4(a)), consistent with experiments indicating a torsionally softer DNA at short distances²⁴. Moreover, its asymptotic value for the long length scale is close to the experimental value obtained from the measurement of Kbp long DNA³⁸ (see Table I). Conversely, the bending persistence length of cgDNA+ more significantly overestimates the consensus experimental value as shown from the data reported in Table I. The excellent overlap between all-atom and cgDNA+ q -stiffnesses suggests that the problem with the bending persistence length is possibly due to the current force fields used in all-atom models³⁹, rather than a problem with the parametrization of cgDNA+.

Finally, as a methodology, the analysis of q -stiffnesses can be very useful in the development of coarse-grained DNA models. A good match of stiffnesses at all q -values with respect to some reference data is an indication of a correct parametrization accounting both for the short- and long distance behavior, as illustrated in the case of the torsional stiffness. Problematic behavior of some degrees of freedom can be spotted more easily from the analysis of q -stiffnesses. This is illustrated in the case of the inter-bp rotation coordinates tilt and twist of cgDNA in Fig. 2(a). From a computational point-of-view, it is important to note that the q -stiffness analysis can be performed reliably on systems of rather small lengths, see Appendix B, since it converges rapidly to its asymptotic values over the whole q -range.

ACKNOWLEDGMENTS

Discussions with E. Skoruppa are gratefully acknowledged. M. S. acknowledges financial support from Fonds Wetenschappelijk Onderzoek (FWO 1102323N).

Appendix A: All-atom and cgDNA(+) simulations

MD all-atom simulations were performed on the two 44 bp sequences given in Table II and as described in Ref. 27. Briefly, Gromacs v.2020.4⁴⁰ and the Amberff99 parmbsc1 force field⁴¹ were used. The TIP-3P water model⁴² was used while non-bonded interactions were cutoff at 1.0 nm and PME Mesh Ewald interactions for electrostatic. The molecules were placed in a dodecahedral box with 2.0 nm spacing on the sides using periodic boundary conditions and a neutralized solution of 150 mM NaCl. The energy was minimized with tolerance of 1000 kJ/mol. A run of 100 ps at 300 K using a velocity rescaling thermostat⁴³ was followed by 100 ps

Sequences

```
CGCTCAAGGGCGAGAATTGGACCTGGCTTACGTCTTAGTACGTA*
GTTAAGTGCCGAACCTAGATCTGACCTAACGGTAAGAGAGTTTCA
```

Table II. The two 44 bp sequences used in the all-atom MD simulations and in the cgDNA/cgDNA+ models to produce the data shown in Figures 2 and 3. The sequence indicated with * was used along with the cgDNA+ model to generate the data in Fig. 5.

at the same temperature using a Parrinello-Rahman barostat⁴⁴ with 1.0 bar pressure. Production runs were performed using the latter barostat and run for 100 ns using a 2 fs time step in a leapfrog integrator. The trajectories were analyzed using the software Curves+⁴⁵, which extracts the twelve rigid base coordinates from atomic configurations. To minimize endpoint effects two base pairs on each end of the molecule were excluded from the analysis.

The data of cgDNA/cgDNA+ models were obtained from Monte Carlo simulations. For cgDNA we used the 2018 2.0 version using the parameter set cgDNAps4. For cgDNA+ we used the parameter set DNA PS2. To obtain the q -stiffnesses of Fig. 2, 3 we sampled 5×10^5 configurations for each of the two 44-mer DNA sequences of Table II. For Fig. 4, 100 different sequences of length 500 bp were used (10^3 samples per sequence), in order to capture to long length scale directly from the correlation functions. As in the all-atom case, the two outer base pairs from each side of the sequences were removed from the analysis of the stiffnesses to reduce end-effects²⁴. The cgDNA/cgDNA+-output for rotational coordinates uses a Cayley vector representation, deviating from the Euler vector representation which was used for the analysis of all-atom MD simulations. Given a Cayley vector $\vec{\theta}$, it can be converted to an Euler vector $\vec{\omega}$ using Eq. (A1)

$$\vec{\omega} = 2 \arctan \left(\frac{|\vec{\theta}|}{2} \right), \frac{\vec{\theta}}{|\vec{\theta}|}. \quad (\text{A1})$$

In order to compare q -stiffnesses from cgDNA/cgDNA+ with those obtained from all-atom simulations, rotational coordinates from cgDNA/cgDNA+ were first converted into Euler vectors prior to the calculation of momentum-space stiffnesses.

Appendix B: Finite size effects

One of the remarkable features we noticed of the q -stiffnesses is their rapid convergence to asymptotic values already for rather short molecules. We illustrate this behavior for tilt, roll and twist stiffnesses in Fig. 6, which shows cgDNA+ calculations for molecules of different lengths (10, 20, 50 and 70 bp). Plotted are the diagonal elements of the 3×3 stiffness matrix describing tilt, roll and twist deformations where all other degrees of freedom are integrated out. Already the 10 bp dataset shows stiffnesses which develop peaks at $q = 0$ which are remarkably close to the long molecule limit values. This suggests that from the analysis of

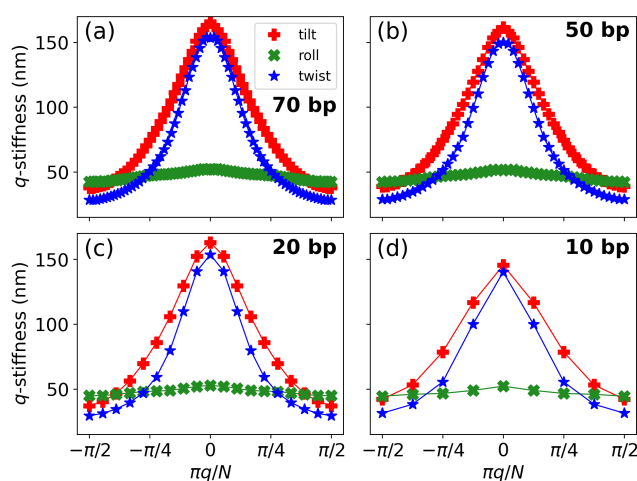


Figure 6. q -stiffnesses for tilt, roll and twist for various DNA lengths. The q -stiffnesses are obtained by considering the three dimensional configuration space spanned by tilt, roll and twist degrees of freedom. In the tilt-roll-twist space, the stiffness matrix becomes a 3×3 -matrix which forms a Schur-complement of the 12×12 matrix in Eq. (5).

the q -stiffnesses one can reliably extract information concerning the elastic behavior, and their length-scale dependence, of very long molecules.

REFERENCES

- ¹M. Pasi *et al.*, “ μ ABC: A systematic microsecond molecular dynamics study of tetranucleotide sequence effects in B-DNA,” *Nucl. Acids Res.* **42**, 12272–12283 (2014).
- ²J. Curuksu, M. Zacharias, R. Lavery, and K. Zakrzewska, “Local and global effects of strong DNA bending induced during molecular dynamics simulations,” *Nucl. Acids Res.* **37**, 3766–3773 (2009).
- ³J. Spiriti, H. Kamberaj, A. M. De Graff, M. Thorpe, and A. Van Der Vaart, “DNA bending through large angles is aided by ionic screening,” *J. Chem. Theor. Comput.* **8**, 2145–2156 (2012).
- ⁴A. Karolak and A. van der Vaart, “Enhanced sampling simulations of DNA step parameters,” *J. Comput. Chem.* **35**, 2297–2304 (2014).
- ⁵A. Peguero-Tejada and A. van der Vaart, “Biasing simulations of DNA base pair parameters with application to propeller twisting in AT/AT, AA/TT, and AC/GT steps and their uracil analogs,” *J. Chem. Inf. Model.* **57**, 85–92 (2017).
- ⁶A. Voorspoels, J. Vreede, and E. Carlon, “Rigid base biasing in molecular dynamics enables enhanced sampling of DNA conformations,” *J. Chem. Theor. Comput.* **19**, 902–909 (2023).
- ⁷T. E. Ouldridge, A. A. Louis, and J. P. Doye, “DNA nanotweezers studied with a coarse-grained model of DNA,” *Phys. Rev. Lett.* **104**, 178101 (2010).
- ⁸O. Henrich, Y. A. G. Fosado, T. Curk, and T. E. Ouldridge, “Coarse-grained simulation of DNA using LAMMPS,” *Eur. Phys. J. E* **41**, 57 (2018).
- ⁹P. D. Dans, A. Zeida, M. R. Machado, and S. Pantano, “A coarse grained model for atomic-detailed DNA simulations with explicit electrostatics,” *J. Chem. Theor. Comput.* **6**, 1711–1725 (2010).
- ¹⁰Y. A. G. Fosado, D. Michieletto, J. Allan, C. Brackley, O. Henrich, and D. Marenduzzo, “A single nucleotide resolution model for large-scale simulations of double stranded DNA,” *Soft Matter* **12**, 9458–9470 (2016).
- ¹¹D. Chakraborty, N. Hori, and D. Thirumalai, “Sequence-dependent three interaction site model for single-and double-stranded DNA,” *J. Chem. Theor. Comput.* **14**, 3763–3779 (2018).
- ¹²S. Assenza and R. Pérez, “Accurate sequence-dependent coarse-grained model for conformational and elastic properties of double-stranded DNA,” *J. Chem. Theor. Comput.* **18**, 3239–3256 (2022).
- ¹³R. Frederickx, T. In’t Veld, and E. Carlon, “Anomalous dynamics of DNA hairpin folding,” *Phys. Rev. Lett.* **112**, 198102 (2014).
- ¹⁴C. Matek, T. E. Ouldridge, J. P. K. Doye, and A. A. Louis, “Plectoneme tip bubbles: Coupled denaturation and writhing in supercoiled DNA,” *Scientific Reports* **5**, 7655 (2015).
- ¹⁵A. Córdoba, D. M. Hinckley, J. Lequieu, and J. J. de Pablo, “A molecular view of the dynamics of dsDNA packing inside viral capsids in the presence of ions,” *Biophys. J.* **112**, 1302–1315 (2017).
- ¹⁶L. Coronel, A. Suma, and C. Micheletti, “Dynamics of supercoiled DNA with complex knots: large-scale rearrangements and persistent multi-strand interlocking,” *Nucl. Acids Res.* **46**, 7533 (2018).
- ¹⁷M. Caraglio, E. Skoruppa, and E. Carlon, “Overtwisting induces polygonal shapes in bent DNA,” *J. Chem. Phys.* **150**, 135101 (2019).
- ¹⁸D. Petkevičiūtė, M. Pasi, O. Gonzalez, and J. Maddocks, “cgDNA: a software package for the prediction of sequence-dependent coarse-grain free energies of B-form DNA,” *Nucl. Acids Res.* **42**, e153–e153 (2014).
- ¹⁹R. Sharma, A. S. Patelli, L. De Bruin, and J. H. Maddocks, “cgNA+ web: A visual interface to the cgNA+ sequence-dependent statistical mechanics model of double-stranded nucleic acids,” *J. Mol. Biol.* , 167978 (2023).
- ²⁰J. Walther, P. D. Dans, A. Balaceanu, A. Hospital, G. Bayarri, and M. Orozco, “A multi-modal coarse grained model of DNA flexibility mappable to the atomistic level,” *Nucl. Acids Res.* **48**, e29–e29 (2020).
- ²¹W. K. Olson *et al.*, “A standard reference frame for the description of nucleic acid base-pair geometry,” *J. Mol. Biol.* **313**, 229–237 (2001).
- ²²A. S. Patelli, *A sequence-dependent coarse-grain model of B-DNA with explicit description of bases and phosphate groups parametrised from large scale Molecular Dynamics simulations*, Ph.D. thesis, EPFL, Lausanne (2019).
- ²³O. Gonzalez, D. Petkeviciute, and J. H. Maddocks, “A sequence-dependent rigid-base model of DNA,” *J. Chem. Phys.* **138** (2013).
- ²⁴E. Skoruppa, A. Voorspoels, J. Vreede, and E. Carlon, “Length-scale-dependent elasticity in DNA from coarse-grained and all-atom models,” *Phys. Rev. E* **103**, 042408 (2021).
- ²⁵M. Segers, A. Voorspoels, T. Sakaue, and E. Carlon, “Mechanical properties of nucleic acids and the non-local twistable wormlike chain model,” *J. Chem. Phys.* **156**, 234105 (2022).
- ²⁶H. Dohnalová and F. Lankaš, “Deciphering the mechanical properties of B-DNA duplex,” *WIREs Comput Mol Sci.* , e1575 (2021).
- ²⁷M. Segers, A. Voorspoels, T. Sakaue, and E. Carlon, “Mechanisms of DNA-mediated allostery,” *Phys. Rev. Lett.* **131**, 238402 (2023).
- ²⁸B. Eslami-Mossallam, H. Schiessel, and J. van Noort, “Nucleosome dynamics: Sequence matters,” *Adv. Colloid Interface Sci.* **232**, 101–113 (2016).
- ²⁹Y. A. Gutiérrez Fosado, F. Landuzzi, and T. Sakaue, “Coarse graining DNA: Symmetry, nonlocal elasticity, and persistence length,” *Phys. Rev. Lett.* **130**, 058402 (2023).
- ³⁰M. Segers, E. Skoruppa, J. A. Stevens, M. Vangilbergen, A. Voorspoels, and E. Carlon, “Comment on “Flexibility of short DNA helices with finite-length effect: From base pairs to tens of base pairs”,” *J. Chem. Phys.* **155**, 027101 (2021).
- ³¹Z. Bryant, M. D. Stone, J. Gore, S. B. Smith, N. R. Cozzarelli, and C. Bustamante, “Structural transitions and elasticity from torque measurements on DNA,” *Nature* **424**, 338–341 (2003).
- ³²J. Lipfert, J. W. Kerssemakers, T. Jager, and N. H. Dekker, “Magnetic torque tweezers: measuring torsional stiffness in DNA and RecA-DNA filaments,” *Nat. Methods* **7**, 977–980 (2010).
- ³³X. Gao, Y. Hong, F. Ye, J. T. Inman, and M. D. Wang, “Torsional Stiffness of Extended and Plectonemic DNA,” *Phys. Rev. Lett.* **127**, 028101 (2021).
- ³⁴J. S. Mitchell, J. Glowacki, A. E. Grandchamp, R. S. Manning, and J. H. Maddocks, “Sequence-dependent persistence lengths of DNA,” *J. Chem. Theory Comput.* **13**, 1539–1555 (2017).
- ³⁵V. A. Bloomfield, D. M. Crothers, and I. Tinoco, *Nucleic acids: Structures, Properties, and Functions* (University Science Books, Sausalito, California).
- ³⁶S. Kim, E. Broströmer, D. Xing, J. Jin, S. Chong, H. Ge, S. Wang, C. Gu, L. Yang, Y. Q. Gao, *et al.*, “Probing allostery through DNA,” *Science* **339**, 816–819 (2013).

- ³⁷G. Rosenblum, N. Elad, H. Rozenberg, F. Wiggers, and H. Hofmann, "Allostery through DNA drives phenotype switching," *Nature Comm.* **12**, 1–12 (2021).
- ³⁸J. Lipfert, G. M. Skinner, J. M. Keegstra, T. Hensgens, T. Jager, D. Dulin, M. Köber, Z. Yu, S. P. Donkers, F.-C. Chou, R. Das, and N. H. Dekker, "Double-stranded RNA under force and torque: Similarities to and striking differences from double-stranded DNA," *Proc. Natl. Acad. Sci. USA* **111**, 15408–15413 (2014).
- ³⁹K. Liebl and M. Zacharias, "The development of nucleic acids force fields: From an unchallenged past to a competitive future," *Biophys. J.* **122**, 2841 (2023).
- ⁴⁰M. Abrahams, T. Murtola, R. Schulz, S. Páll, J. Smith, B. Hess, and E. Lindahl, "GROMACS: high performance molecular simulations through multi-level parallelism from laptops to supercomputers," *SoftwareX* **1-2**, 19–25 (2015).
- ⁴¹I. Ivani *et al.*, "Parmbsc1: a refined force field for DNA simulations," *Nat. Methods* **13**, 55–58 (2016).
- ⁴²W. L. Jorgensen, J. Chandrasekhar, J. D. Madura, R. W. Impey, and M. L. Klein, "Comparison of simple potential functions for simulating liquid water," *J. Chem. Phys.* **79**, 926–935 (1983).
- ⁴³G. Bussi, D. Donadio, and M. Parrinello, "Canonical sampling through velocity rescaling," *J. Chem. Phys.* **126**, 014101 (2007).
- ⁴⁴M. Parrinello and A. Rahman, "Polymorphic transitions in single crystals: A new molecular dynamics method," *J. Appl. Phys.* **52**, 7182–7190 (1981).
- ⁴⁵R. Lavery, M. Moakher, J. Maddocks, D. Petkeviciute, and D. Zakrzewska, "Conformational analysis of nucleic acids revisited: Curves+," *Nucl. Acids Res.* **37**, 5917–5929 (2009).